



Superior Vis light photo-catalytic efficiency for remediation of gaseous toluene using $\text{FeWO}_4/\text{g-C}_3\text{N}_4$ direct Z system

Reda M. Mohamed^{a,b,*}, Detlef W. Bahnemann^{c,d}, Amal S. Basaleh^a, Razan H. Gadah^a

^aDepartment of Chemistry, Faculty of Science, King Abdulaziz University, P.O. Box: 80203, Jeddah 21589, Saudi Arabia, emails: redama123@yahoo.com (R.M. Mohamed), amalbasaleh1@gmail.com (A.S. Basaleh), razanqadah1@gmail.com (R.H. Gadah)

^bAdvanced Materials Department, Central Metallurgical R&D Institute, CMRDI, P.O. Box: 87, Helwan, Cairo 11421, Egypt

^cPhotocatalysis and Nanotechnology Unit, Institute of Technical Chemistry, Leibniz University, Callinstr. 3, 30167 Hannover, Germany, email: Bahnemann@iftc.uni-hannover.de (D.W. Bahnemann)

^dPhotoactive Nanocomposite Materials, Saint-Petersburg, State University, Ulyanovskaya Str, Peterhof, Saint-Petersburg, 198504, Russia

Received 5 August 2019; Accepted 23 November 2019

ABSTRACT

In this investigation, removal of gaseous toluene has been performed adopting $\text{FeWO}_4/\text{g-C}_3\text{N}_4$ composites. The collected data and analyses have indicated that a combination of the two components ($\text{g-C}_3\text{N}_4$ and FeWO_4) in the mode of $\text{FeWO}_4/\text{g-C}_3\text{N}_4$ composite showed better catalytic efficiency for gaseous toluene remediation compared to that of the individual constituents themselves. The performed enhancement has been done through the direct Z-scheme tool. In this system, as the result of the special amalgamation between $\text{g-C}_3\text{N}_4$ and FeWO_4 , there was a combination of the photo-excited electrons from the conduction band (C.B.) of the FeWO_4 with the photo-excited holes from the valence band (V.B.) of the $\text{g-C}_3\text{N}_4$ whereas, the holes in the V.B. of the FeWO_4 and the electrons in C.B. of the $\text{g-C}_3\text{N}_4$ were preserved. And so, the powerful quantity of accessible holes and electrons could be produced via the synthesized $\text{FeWO}_4/\text{g-C}_3\text{N}_4$ composite, which by their role, contributed strongly to the photo-catalytic destruction of the gaseous toluene although beneath visible light. The equal molar ratios of FeWO_4 and $\text{g-C}_3\text{N}_4$ (1Fe/1C material) have proven to possess the greatest photo-catalytic remediation of gaseous toluene. Gaseous toluene has been removed and mineralized adopting the synthesized 1Fe/1C material with percentages of 96.6% and 99.6%, respectively. In addition, the synthesized $\text{FeWO}_4/\text{g-C}_3\text{N}_4$ composite showed great stability all over the removal process of toluene.

Keywords: FeWO_4 ; $\text{g-C}_3\text{N}_4$; Remediation of gaseous toluene; Visible light.

1. Introduction

One of the considerable gaseous pollutants is the group of volatile organic compounds (VOCs), these gaseous compounds may be produced through diverse developments, combustion of natural gas and building goods. The crucial problem of the VOCs is their hazardous consequences for human beings [1–6]. Gaseous toluene, one of the VOCs, may be introduced to blood through the skin, gastrointestinal

tract, and lung. And so, it assembles in the liver, brain and other tissues bringing about central nervous system abjection [7,8]. Alternative regimes have been expanded to manage VOCs such as photo-catalytic, chemical, and bio-filtration destructive manners along with adsorption, condensation, and absorption non-destructive manners [2,9–15]. The greatest catalytic efficacy, mild operation actions and cheapness accomplish the photocatalytic oxidation (PCO) manner to be a highly advanced manner for the pollutant remediation.

* Corresponding author.

TiO₂, ZnO, and SnO₂ have been reported as successful photo-catalysts for pollutant removal. The large bandgap energy of such photo-catalysts makes their utilization for photo-catalytic applications to be restricted in the ultraviolet (UV) zone, which by its role, brings about energy decay [16–21]. To conquer the mentioned imperfections of the large bandgap energy compounds, there was a need to fabricate novel photo-catalyst that could respond positively to the visible (Vis) light region [22]. g-C₃N₄ has been nominated to be a material that responds to the Vis light zone. In addition, it possesses great thermal and chemical stabilities. g-C₃N₄ has been established for numerous applications such as the photocatalytic transformation of CO₂, remediation of various pollutants in addition to O₂ and/or H₂ production from water breaking beneath Vis light [23–28]. Unsuccessfully, g-C₃N₄ has featured with great re-consolidation speed of the photo-excited holes and electrons as a result of its substantial Coulombic attraction and so, the applications of these types of photo-catalysts were restricted and limited [27]. Several attempts have been performed in order to enhance the separation of the segregation efficacy of the photo-excited electrons and positive holes. One of the most effective approaches to such enhancement is the consolidation of g-C₃N₄ with another semiconductor to synthesize heterojunction composite. A hetero-junction made of type II g-C₃N₄/TiO₂ nano-composite has been fabricated and tested adequately for photocatalytic hydrogen production beneath Vis light. Nevertheless, some type II heterojunctions possess fluctuating bandgap energy and subsequent undesirable redox potential failure [29]. Recently, the Z direct scheme system (a system that depends on rational consolidation between two photo-catalysts of low bandgap energies) has been innovated. In this scheme, the positive holes (h⁺) with lesser redox capability in the V.B. of the first photo-catalyst are re-associated with the photo-excited electrons of the C.B. of the second catalyst whereas, the photo-excited electrons with energetic reduction capability in the C.B. of the first photo-catalyst as well as the positive holes with energetic oxidation capability in the V.B. of the second photo-catalyst are retained. This mechanism enlarges the redox capabilities of the photo-catalysts ingredients and also it promotes the charge separation performance. Various photo-catalysts possessing Z direct scheme (installed by a combination of C₃N₄ with other photocatalysts) have been addressed in the former years.

Some Z direct scheme photocatalysts have been disclosed such that g-C₃N₄ was coupled with one of the following semiconductors; WO₃, BiPO₄, SnNb₂O₆, BiVO₄, MoS₂, Ag₂CrO₄, etc. [16,30–33]. It was discovered that the Z direct scheme photo-catalysts made of g-C₃N₄ combined with other semiconductors possessed more immense catalytic efficiencies in comparison to that of the individual g-C₃N₄ itself.

As long as the attractive catalytic, magnetic and optical aspects, diverse metal tungstates (NiWO₄, Bi₂WO₆, CoWO₄ and CuWO₄) have been inspected towards numerous operations [34–37]. It has been revealed that FeWO₄, owing to its low bandgap energy, has been covered in various areas such as super-capacitors, sensors, and catalysts [38]. In addition, FeWO₄ has been recorded as a highly efficient photocatalyst for organic pollutants remediation [34]. Nevertheless, the

photocatalytic efficiency of FeWO₄ is somewhat little as a result of the great velocity of the re-consolidation of the photo-excited electrons and the positive holes.

The present work investigates the combination of FeWO₄ and g-C₃N₄ to fabricate an exceptional photo-catalyst possessing Z direct scheme that generates a sufficient amount of electrons and holes beneath Vis light in addition to the production of electron/holes couples of great redox capabilities which affects greatly destruction of toluene.

2. Experimental section

2.1. Materials fabrication

All chemicals used for preparation are of analytical grade. FeWO₄ has been fabricated via the utilization of two precursors (Na₂WO₄·2H₂O and (NH₄)₂Fe(SO₄)₂·6H₂O). Bi-distilled water having polyethylene glycol (2%) was applied to dissolve Na₂WO₄·2H₂O. After that, (NH₄)₂Fe(SO₄)₂·6H₂O solution was introduced drop-wisely to Na₂WO₄·2H₂O solution applying vigorous leading to the formation of darkened brown residue. The previous system was centrifuged to gather the formed ppt which was cleaned and washed via ethanol and bi-distilled water many intervals. Finally, the resultant yield was kept to dry for about 6 h at 150°C and then fired for 4 h at 500°C to attain FeWO₄.

To fabricate the novel FeWO₄/g-C₃N₄ photocatalyst that possesses a direct Z scheme, a calculated quantity of the previously-fabricated FeWO₄ was admixed with melamine and ground to attain homogenous blend. Then, the ground homogenous blend was burnt for 3 h at 500°C to attain the required FeWO₄/g-C₃N₄ photo-catalyst that possesses a direct Z scheme. FeWO₄/g-C₃N₄ photo-catalysts of molar ratios 1:1, 2:1 and 1:2 were fabricated by governing the FeWO₄/melamine ratios.

The previously mentioned steps were rerun avoiding the utilization of the fabricated FeWO₄ to melamine to attain g-C₃N₄ material.

2.2. Identification of the fabricated materials

X-ray diffraction (XRD) diffractograms of the fabricated photo-catalysts (FeWO₄, g-C₃N₄, and FeWO₄/g-C₃N₄) have been achieved using XRD analyzer of Bruker AXS model. Whereas, the transmission electron microscopy (TEM) photographs of the fabricated FeWO₄/g-C₃N₄ photocatalysts have been performed via the JEOL JEM-1230 TEM device.

Additionally, the specific surface areas of the fabricated specimens were estimated from the Brunauer–Emmett–Teller (BET) equation after adopting adsorption–desorption isotherms (utilizing the Chromatech apparatus-Nova 2000 series at 77 K). UV/Vis/Near-Infrared spectrophotometer has been applied to characterize the optical absorption features of the fabricated photo-catalysts.

Additionally, a fluorescence spectrophotometer (wavelength at 350 nm) was adopted to characterize the photoluminescence spectra (PL) of the fabricated specimens.

Finally, the photo-electrochemical features of the fabricated specimens were performed via the conventional cell consisting of three electrodes. The cell under investigation

was made of the following: (i) reference electrode (Ag/AgCl), (ii) counter electrode (Pt), (iii) the electrolyte (0.5 M Na_2SO_4 solution of pH = 6.8) and (iv) working electrode (prepared by scattering the required photo-catalyst in dimethylformamide (DMF) having a proportion of 1 mg specimen: 0.1 mL DMF and the suspension was agitated via ultrasonic for slurry production). To perform the photo-electrochemical test, Vis luminous ranging from 400 nm up to 700 nm was generated via Xe lamp (1,000 W).

2.3. Removal tests

1 L quartz photo-reactor has been adopted to perform the photo-catalytic remediation test of gaseous toluene. 100 W Xe-arc lamps (two lamps) were used as a source of Vis light and the lamps were situated at the base and the top of the reaction enclosure.

A sample of 0.5 g of the fabricated photo-catalyst was dispersed homogeneously on the bottom of the reactor. Fabricated gaseous medium (80% N_2 and 20% O_2 containing 1,000 ppm toluene) has been supplied as input gas. The original relative humidity and toluene dose of the inlet was 50% and 50 ppm, respectively.

The adsorption/desorption equilibrium has been attained for the input gas over the fabricated photo-catalyst to be 60 min in the dark. Then, the photo-catalytic destruction process has been permitted after turning on the Vis light lamps. 0.5 mL gas was eliminated from the reaction medium (after every 20 min interval) to be analyzed via a gas chromatography device. Recognizing CO , O_2 , and N_2 have been achieved applying 5A column whereas, recognizing CO_2 and hydrocarbons been achieved via the Porapak Q column. The initial time of reaction has been recorded as the point of introducing toluene to the reaction medium.

The following equations could be applied to estimate both mineralization degree and remediation performance of toluene gas.

$$\text{Mineralization degree} = \frac{C_t(\text{CO}_2)}{7(C_0 - C_t)} \times 100 \quad (1)$$

$$\text{Remediation performance}(\%) = \frac{C_0 - C_t}{C_0} \times 100 \quad (2)$$

where C_0 is the initial concentration of toluene (50 ppm) at zero time; C_t is the concentration of gaseous toluene at several intervals; $C_t(\text{CO}_2)$ is the concentration CO_2 at any time.

3. Results and discussion

3.1. Material identifications

3.1.1. Phase composition and surface area

The XRD diffractograms of the fabricated specimens (FeWO_4 , $\text{g-C}_3\text{N}_4$, and 1Fe/1C specimens) are exhibited in Fig. 1. The XRD diffractograms of the fabricated FeWO_4 illustrated the principle patterns that match the presence of crystallographic phases of the monoclinic FeWO_4 phase. Whereas, the conjugated double bonds for graphitic material (fabricated $\text{g-C}_3\text{N}_4$) has been proven by the presence

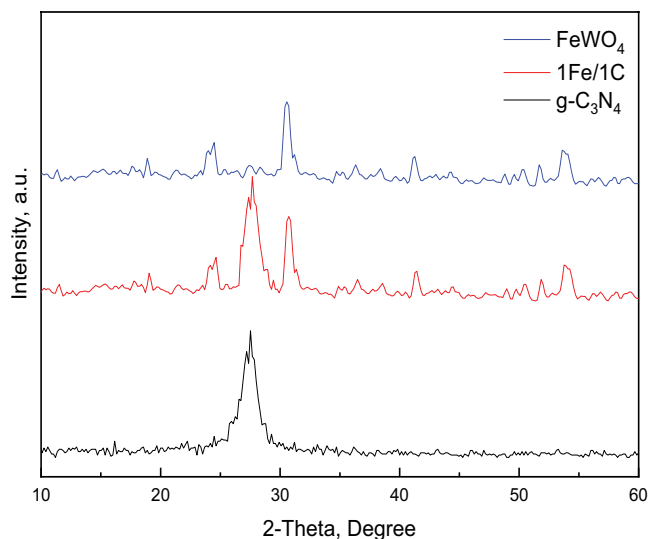


Fig. 1. XRD diffractograms of FeWO_4 , $\text{g-C}_3\text{N}_4$, and $\text{FeWO}_4/\text{g-C}_3\text{N}_4$ samples.

of the diffraction pattern at $2\theta = 27.5^\circ$ [39]. Moreover, the XRD diffractograms of the 1Fe/1C specimens illustrate that XRD patterns of $\text{FeWO}_4/\text{g-C}_3\text{N}_4$ specimens are in agreement with those of both FeWO_4 and the $\text{g-C}_3\text{N}_4$ which confirm the presence of both phases within the resultant photo-catalyst ($\text{FeWO}_4/\text{g-C}_3\text{N}_4$).

An interesting observation has been recorded by the shift of the (002) peak of the graphitic material in $\text{FeWO}_4/\text{g-C}_3\text{N}_4$ towards a larger angle correlated with that of neat $\text{g-C}_3\text{N}_4$. Such findings could be attributed to the decreasing of the interlayer spaces amid $\text{g-C}_3\text{N}_4$ layers because of nitrogen defects increasing in the fabricated photo-catalyst.

Fig. 2a presents the TEM micrograph of the 1Fe/1C specimen whereas; high-resolution transmission electron microscopy (HRTEM) micrograph of an elected area in the TEM micrograph of the 1Fe/1C is exhibited (Fig. 2b). Nanoparticles of FeWO_4 are recognized to be scattered on the nanolayer of $\text{g-C}_3\text{N}_4$. In addition, shining lattice fringes of the FeWO_4 are displayed in the HRTEM micrograph of 1Fe/1C specimens (Fig. 2b) [34]. The detected successful amalgamation between FeWO_4 and $\text{g-C}_3\text{N}_4$ was the fundamental argumentation of the creation of the Z direct scheme photo-catalyst that manipulated to the enhancement of charge separation between both constituents.

Fig. 3 presents the Raman spectra of the fabricated specimens (FeWO_4 , $\text{g-C}_3\text{N}_4$, and $\text{FeWO}_4/\text{g-C}_3\text{N}_4$ specimens). Two intense peaks are discovered at 426 and 355 cm^{-1} in the Raman spectra of FeWO_4 material [39,40]. Presence of W–O bond stretching could be derived by the existence of the band at 426 cm^{-1} [39]. Whereas, the spectrum of $\text{g-C}_3\text{N}_4$ specimen exhibits intense peaks at 812 and 718 cm^{-1} [41]. Finally, the illustrated spectra of Fig. 3 indicate that the fabricated $\text{FeWO}_4/\text{g-C}_3\text{N}_4$ sample displays nearly all the common spectral bands of both FeWO_4 and $\text{g-C}_3\text{N}_4$. Nevertheless, the displacement of the peaks characterizing FeWO_4 in the fabricated $\text{FeWO}_4/\text{g-C}_3\text{N}_4$ sample towards larger values might be connected with the combination of FeWO_4 and $\text{g-C}_3\text{N}_4$ [42,43].

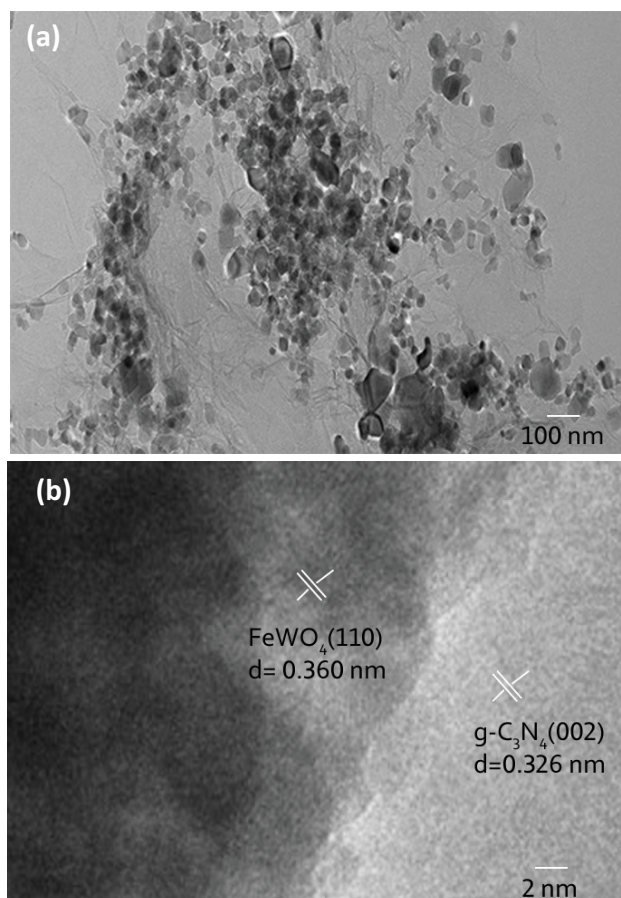


Fig. 2. TEM (a) and HRTEM (b) images of the $\text{FeWO}_4/\text{g-C}_3\text{N}_4$ sample.

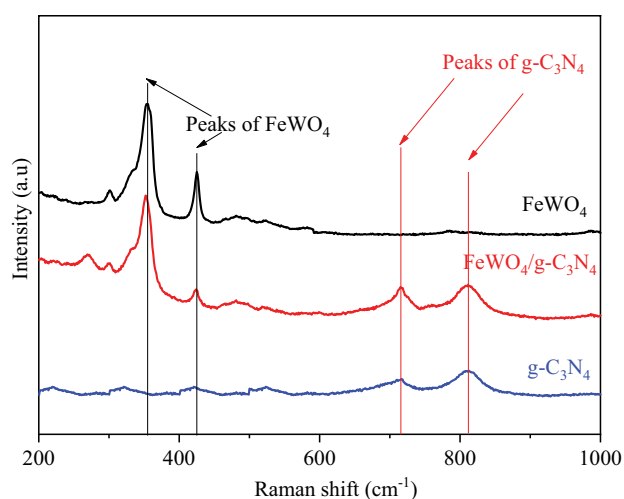


Fig. 3. Raman spectra of FeWO_4 , $\text{g-C}_3\text{N}_4$, and $\text{FeWO}_4/\text{g-C}_3\text{N}_4$ samples.

The high-resolution spectra of the C1s of the fabricated graphitic carbon nitride and $\text{FeWO}_4/\text{g-C}_3\text{N}_4$ specimens are exhibited in Figs. 4a and b, respectively. The data of Fig. 4 illustrates that the resultant spectra are adapted by Gaussian multi-peak features to identify the various

attitudes of carbon in the fabricated specimens. Two recognizable peaks are observed in the C1s spectra of the fabricated graphitic carbon nitride. The accidental hydrocarbon from the instrument itself may be the reason for the appearance of the first peak (at 284.8 eV). On the other hand, the carbon of sp^2 hybridization in N-incorporating aromatic arrangement N-C=N is the reason for the appearance of the second peak (at 288.3 eV) [44]. Whereas, X-ray photoelectron spectroscopy (XPS) spectra of C1s of the $\text{FeWO}_4/\text{g-C}_3\text{N}_4$ exhibits an unusual peak at 289.2 eV in the XPS spectra of C1s assigned to $\text{FeWO}_4/\text{g-C}_3\text{N}_4$. This peak is assigned to the existence of a C–O bond, designed from O atoms of FeWO_4 particles and C atoms of $\text{g-C}_3\text{N}_4$ [45]. The habitation of the C–O bond is a clear illustration that the mood of connection between FeWO_4 and $\text{g-C}_3\text{N}_4$ is a Z-direct pattern mood and isn't a physical one. We conclude from the XPS analysis that FeWO_4 and $\text{g-C}_3\text{N}_4$ were associated through the formation of a tight interface along with a chemical bond between O of FeWO_4 and C of $\text{g-C}_3\text{N}_4$ but not through the physical.

Specific surface areas of the fabricated specimens are tabulated in Table 1. It is clear from the data of Table 1 that the specific surface areas of 72.0, 20.0, 84.0, 88.0, and $75.0 \text{ m}^2/\text{g}$ are assigned to the $\text{g-C}_3\text{N}_4$, FeWO_4 , 1Fe/1C, 1Fe/2C, and 2Fe/1C specimens, respectively. The clear observation from these data is the bigger value of the specific area of the $\text{FeWO}_4/\text{g-C}_3\text{N}_4$ sample correlated to those of $\text{g-C}_3\text{N}_4$ and FeWO_4 . This finding clarifies that the association of FeWO_4 and $\text{g-C}_3\text{N}_4$ via Z-direct pattern contributes positively to the enlargement of the area of the resultant $\text{FeWO}_4/\text{g-C}_3\text{N}_4$. Such a conclusion affords more active sites on $\text{FeWO}_4/\text{g-C}_3\text{N}_4$ correlated to those of the individual photo-catalysts leading to improved photocatalytic efficiency [46].

3.1.2. Optical characteristics

UV–Vis absorption spectra of the fabricated specimens ($\text{g-C}_3\text{N}_4$, FeWO_4 , and $\text{FeWO}_4/\text{g-C}_3\text{N}_4$) are exhibited in Fig. 5 and their analogous band gaps are tabulated in Table 1. It is achieved from the data that the band gaps of $\text{g-C}_3\text{N}_4$ and FeWO_4 are 2.70 and 1.80 eV, respectively and they absorbed light in UV and visible ranges. It is concluded from the illustration of Fig. 5 that $\text{FeWO}_4/\text{g-C}_3\text{N}_4$ fabricated specimens absorb the higher quantity of Vis light correlated to those of the individual FeWO_4 and $\text{g-C}_3\text{N}_4$ specimens. On the other hand, it is indicated that the values 1.95, 2.02, and 2.15 eV are assigned as the band gaps of g-1Fe/1C , 1Fe/2C, and 2Fe/1C specimens, respectively. It is well known that the difference in energy between conduction band (C.B.) minimal and valence band (V.B.) maximal might be deduced from the bandgap data of the photocatalyst. And so, 0.91 and -1.13 eV values are assigned as the C.B. minimal values of the FeWO_4 and $\text{g-C}_3\text{N}_4$, respectively. Furthermore, the resultant HRTEM observations pointed out that there is an intimate combination between FeWO_4 and $\text{g-C}_3\text{N}_4$. All previous conclusions assure the successful integration of FeWO_4 and $\text{g-C}_3\text{N}_4$ to create a direct Z pattern structure (Fig. 6). In addition, the consistent V.B. maximal energy values of the fabricated FeWO_4 and $\text{g-C}_3\text{N}_4$ were 2.71 and 1.57, respectively. And so, the values of the C.B. minimal of the fabricated FeWO_4 and $\text{g-C}_3\text{N}_4$ were 0.91 and -1.13 eV , respectively. The individual semiconductors that possess narrow

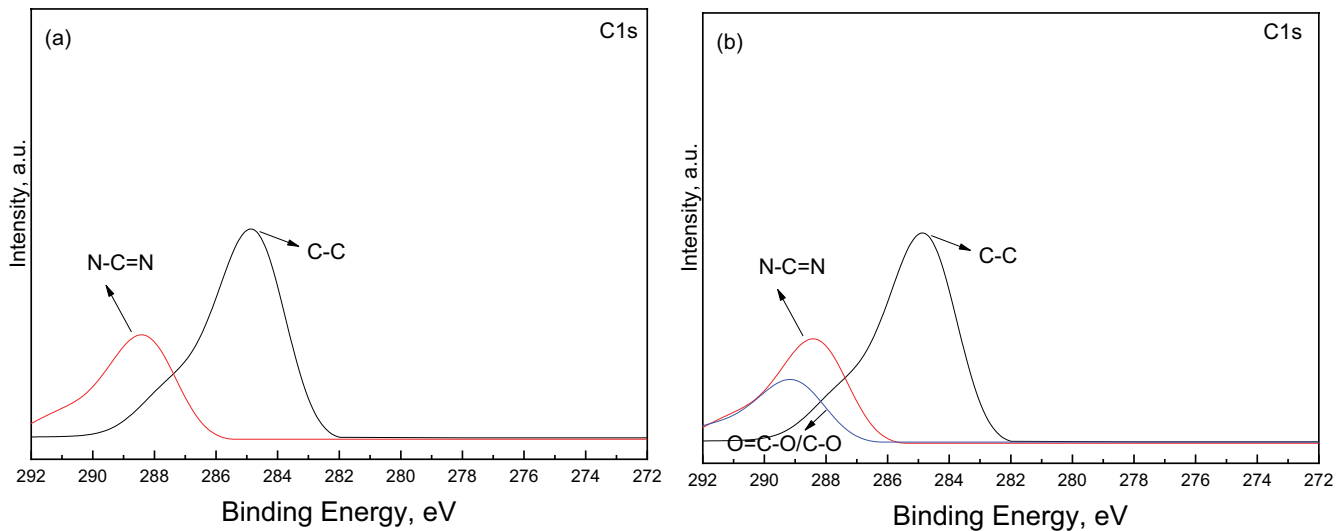


Fig. 4. High-resolution spectra of the C1s of the fabricated graphitic carbon nitride (a) and $\text{FeWO}_4/\text{g-C}_3\text{N}_4$ (b) samples.

Table 1

Surface areas, bandgap energies, maximum removal efficiency and mineralization degree of toluene of the $\text{g-C}_3\text{N}_4$, FeWO_4 , and $\text{FeWO}_4/\text{g-C}_3\text{N}_4$

Sample	BET surface area, m^2/g	Band gaps (eV)	Maximum removal efficiency (%)	Maximum mineralization degree (%)
$\text{g-C}_3\text{N}_4$	72.0	2.70	20.0	23.0
FeWO_4	20.0	1.80	40.0	43.0
1Fe/1C	84.0	1.95	96.6	99.6
2Fe/1C	75.0	2.02	85.0	83.0
1Fe/2C	88.0	2.15	70.0	73.0

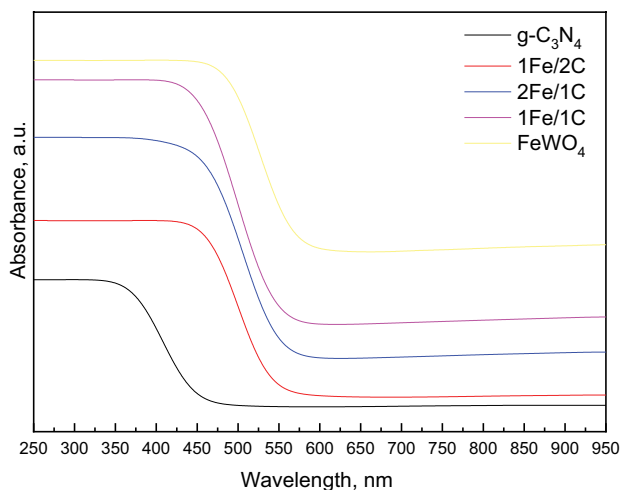


Fig. 5. UV-Vis absorption spectra of FeWO_4 , $\text{g-C}_3\text{N}_4$, and $\text{FeWO}_4/\text{g-C}_3\text{N}_4$ samples.

bandgap values (FeWO_4 or $\text{g-C}_3\text{N}_4$) might absorb Vis light needed for electrons to be excited from the V.B. to the C.B. and holes in the V.B. are left. Though, rapid re-consolidation between the photoexcited electrons and holes would occur. Whereas, In the settled Z direct pattern arrangement,

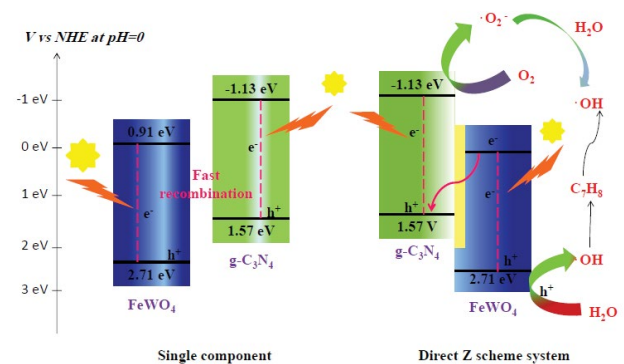


Fig. 6. Direct Z scheme system mechanism of $\text{FeWO}_4/\text{g-C}_3\text{N}_4$ sample.

considering the close amalgamation amid FeWO_4 and $\text{g-C}_3\text{N}_4$, V.B. photoexcited holes in $\text{g-C}_3\text{N}_4$ favors to associate with the C.B. photoexcited electrons in FeWO_4 conserving the presence of the V.B. holes in FeWO_4 and the C.B. electrons in $\text{g-C}_3\text{N}_4$ (Fig. 6).

In conclusion, in the settled Z direct scheme arrangement ($\text{FeWO}_4/\text{g-C}_3\text{N}_4$), the Vis light could be employed to energize electrons from FeWO_4 C.B. to the $\text{g-C}_3\text{N}_4$. And so, Vis light absorption by $\text{FeWO}_4/\text{g-C}_3\text{N}_4$ specimens will be preferable

correlated to those of the individual $g\text{-C}_3\text{N}_4$ or $g\text{-C}_3\text{N}_4$ specimens [46–52]. Fig. 5 also illustrates that 1C/1N specimen could absorb the highest amount of Vis light among those fabricated $\text{FeWO}_4/g\text{-C}_3\text{N}_4$ specimens.

Fig. 7 illustrates that $\text{FeWO}_4/g\text{-C}_3\text{N}_4$ specimens possess smaller PL peak intensities compared to those of the individual FeWO_4 or $g\text{-C}_3\text{N}_4$ semiconductors. These findings demonstrate that through the Z scheme mechanism there will be a definite delaying for the lifetimes of photoexcited holes and electrons or by other meaning, there will be lowering for the re-consolidation velocity of the photoexcited holes and electrons of the specimens. Furthermore, the outstanding establishment of $g\text{-C}_3\text{N}_4$ and FeWO_4 specimens activated the formation of an unusual band of red displacement in the PL spectra of all specimens. Definitely, PL results illustrated that the re-consolidation velocity of photo-excited holes and electrons in the 1Fe/1C was the smallest amid the fabricated $\text{FeWO}_4/g\text{-C}_3\text{N}_4$ composites.

3.1.3. Photo-electrochemical characteristics

Fig. 8 exhibits the photocurrent feedback of the fabricated $g\text{-C}_3\text{N}_4$, FeWO_4 and $\text{FeWO}_4/g\text{-C}_3\text{N}_4$ specimens beneath dark and Vis light settings at 0 V as applied potential (vs. NHE). It is shown from the data of Fig. 8 that no electrons or holes were produced unless a light is provided. Nevertheless, as long as Vis light was granted the fabricated specimens ($g\text{-C}_3\text{N}_4$, FeWO_4 and $\text{FeWO}_4/g\text{-C}_3\text{N}_4$) displayed definite values of photocurrent response as a result of the production of the plentiful quantity of holes and electrons. It is clear from the data of Fig. 8 that $\text{FeWO}_4/g\text{-C}_3\text{N}_4$ specimens possess larger photocurrent responses as compared to those of the individual $g\text{-C}_3\text{N}_4$ and FeWO_4 specimens. Electrons from the V.B. could be excited to the C.B. of Both $g\text{-C}_3\text{N}_4$ and FeWO_4 after absorption of Vis light. It was previously stated that photo-excited holes in the V.B. of the $g\text{-C}_3\text{N}_4$ favor the association with the photo-energetic electrons in the C.B. of the FeWO_4 . The presence of such a system ($\text{FeWO}_4/g\text{-C}_3\text{N}_4$) activates the conservation of holes in the V.B. of the FeWO_4 and electrons in the C.B. of the $g\text{-C}_3\text{N}_4$ and/or the production of a large number of accessible electrons and holes correlated

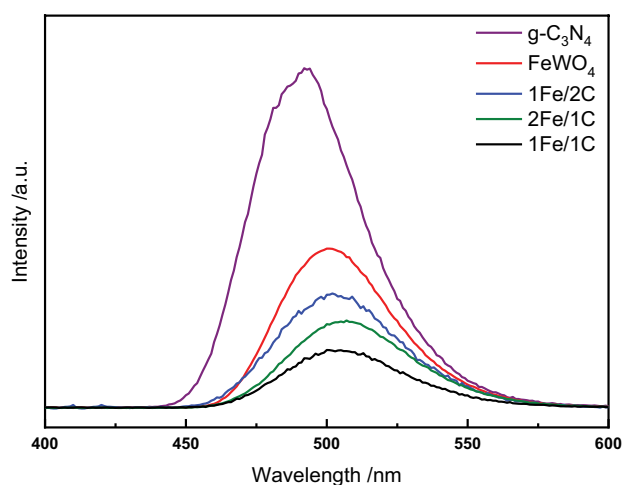


Fig. 7. PL spectra of FeWO_4 , $g\text{-C}_3\text{N}_4$ and $\text{FeWO}_4/g\text{-C}_3\text{N}_4$ samples.

to those in the individual $g\text{-C}_3\text{N}_4$ or FeWO_4 specimens. This consequence could explain the greater photocurrent response values of the $\text{FeWO}_4/g\text{-C}_3\text{N}_4$ specimens correlated to those of the individual $g\text{-C}_3\text{N}_4$ and FeWO_4 specimens.

It is clear also from the data of Fig. 8 that 1Fe/1C specimen possesses the largest photocurrent response among other fabricated $\text{FeWO}_4/g\text{-C}_3\text{N}_4$ specimens.

3.2. Toluene remediation

3.2.1. Remediation mechanism

First, a blank examination for a synthetic gaseous medium without toluene and photo-catalyst has been achieved to assure that any carbon-containing products would be originated from toluene. The remediation efficacy and mineralization extent of toluene by a photo-catalyst are exhibited in Fig. 9. The examination was established after the first 1 h beneath a dark and after the later 2 h beneath Vis light circumstances.

Fig. 9 illustrates that beneath a dark definite quantity of toluene could be eliminated by the photo-catalysts beneath dark although the absence of carbon dioxide in outlet gas after the photocatalytic destruction of toluene. This finding assures that toluene has been removed via adsorption and/or its mineralization extent was 0%. The maximal remediation efficiencies of toluene were found to be 4.2%, 10.4%, 14.5%, 12.5%, and 15.7% by adsorption of the FeWO_4 , $g\text{-C}_3\text{N}_4$, 1Fe/1C, 2Fe/1C, and 1Fe/2C, respectively. It can be concluded that as the surface area of the photo-catalyst increases the removal efficiency increases.

On the other hand, the following observations have been detected after application of the Vis light: (i) indicative quantity of CO_2 has been distinguished in the outlet gas and (ii) the remediation efficiency of toluene was greatly increased as the result of Vis light application. These findings assure the occurrence of a photo-catalytic destruction mechanism for toluene under Vis light. Table 1 tabulates the mineralization extent and the maximal remediation efficiency of toluene by the fabricated specimens. Incident Vis light could be absorbed via the fabricated specimens and

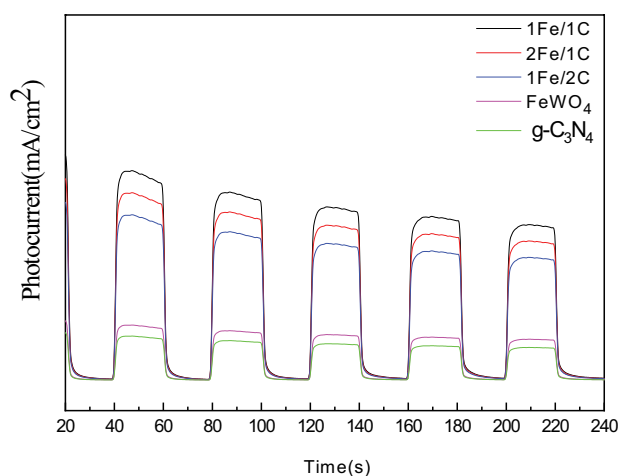


Fig. 8. Photocurrent feedback of FeWO_4 , $g\text{-C}_3\text{N}_4$ and $\text{FeWO}_4/g\text{-C}_3\text{N}_4$ samples.

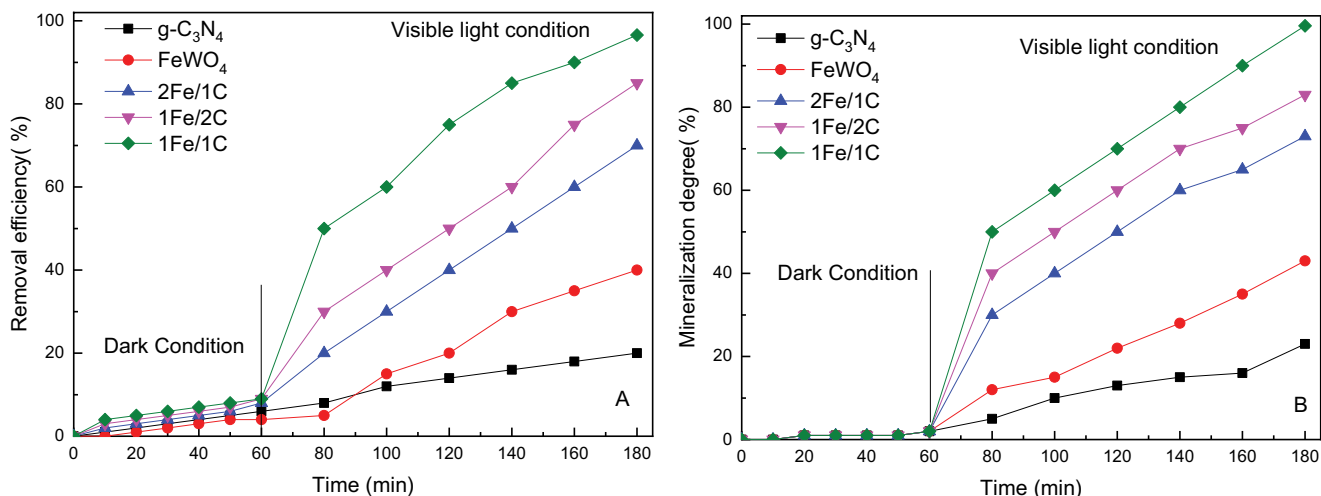
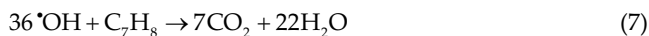
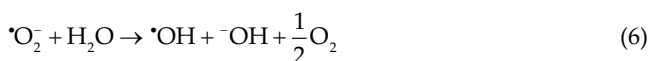
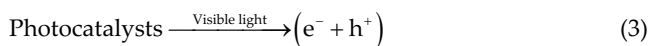


Fig. 9. Remediation efficiency (a) and mineralization extent (b) of toluene by FeWO_4 , $\text{g-C}_3\text{N}_4$, and $\text{FeWO}_4/\text{g-C}_3\text{N}_4$ samples.

electron-hole pairs have been produced. And so, the generated holes and electrons reacted with water and/or oxygen molecules to generate hydroxyl radicals. And so, toluene has been oxidized by these generated hydroxyl radicals which act as strong oxidizing agents and the products of oxidation are CO_2 and H_2O .

The mechanism of the photocatalytic destruction of toluene by the fabricated specimens is illustrated by the following steps [51,52].



All results confirm that the Z scheme mechanism contributed strongly to the higher rate of the photocatalytic destruction of toluene by $\text{FeWO}_4/\text{g-C}_3\text{N}_4$ specimens correlated to those of the individual $\text{g-C}_3\text{N}_4$ and FeWO_4 materials.

The attained results confirmed that the 1Fe/1C specimen exhibited the greatest photo-catalytic destruction efficiency of toluene among all fabricated $\text{FeWO}_4/\text{g-C}_3\text{N}_4$ specimens. The maximal remediation efficacy and mineralization extent of toluene via 1Fe/1C were found to be 96.6% and 99.6%, respectively. Table 2 shows a comparison of different catalysts for PCO of toluene.

Fig. 9 illustrates that in the initial 30 min of Vis light illumination (short period of illumination), the gaseous toluene remediation efficacy by $\text{g-C}_3\text{N}_4$ material was much bigger than that of the FeWO_4 material. This attributed to the dual nature of the photo-catalytic destruction mechanism of toluene remediation (adsorption and degradation). Since $\text{g-C}_3\text{N}_4$ material adsorbs toluene effectively than FeWO_4 does, this leads to greater toluene remediation efficacy when $\text{g-C}_3\text{N}_4$ is adopted compared to that when FeWO_4 is adopted. On the other hand, after 40 min of Vis light illumination (long period of illumination), an inverse consequence was monitored. Gaseous toluene was principally eliminated via the photo-catalytic destruction development. In this situation, both specimens (FeWO_4 and $\text{g-C}_3\text{N}_4$) have the capability to absorb the incident Vis light to generate holes and electrons existing in the V.B. and C.B., respectively.

The P.E. of the V.B. of the $\text{g-C}_3\text{N}_4$ is about +1.57 V. This potential energy value isn't enough for holes to be associated with water to create hydroxyl radicals (Eq. (4)). Consequently, hydroxyl radicals could be originated exclusively from electrons in the C.B. of the $\text{g-C}_3\text{N}_4$ (Eqs. (4)–(6)).

Table 2
Comparison of different catalysts for photocatalytic oxidation of toluene

Photocatalyst	Reaction condition	Removal (%)
Flower-like Bi_2WO_6 [53]	Catalyst (50 mg), toluene (8 mmol), O_2 , $\lambda \geq 400$ nm, 5 h	96
$\text{Pd}/\text{Bi}_2\text{WO}_6$ [54]	Catalyst (50 mg), toluene (1 mL), $\lambda > 400$ nm, 5 h	90
$\text{W}_{18}\text{O}_{49}$ nanowires [55]	Catalyst (50 mg), toluene (10 mL), $\lambda \geq 420$ nm, 20 h	92
Bi doped $\text{Bi}_2\text{MoO}_6\text{-Bi}_2\text{Mo}_3\text{O}_{12}$ [56]	Catalyst (50 mg), toluene (0.1 mmol), O_2 , $\lambda \geq 400$ nm, 5 h	98.5
1Fe/1C this work	Catalyst (50 mg), toluene (50 ppm), O_2 , $\lambda \geq 420$ nm, 3 h	96.6

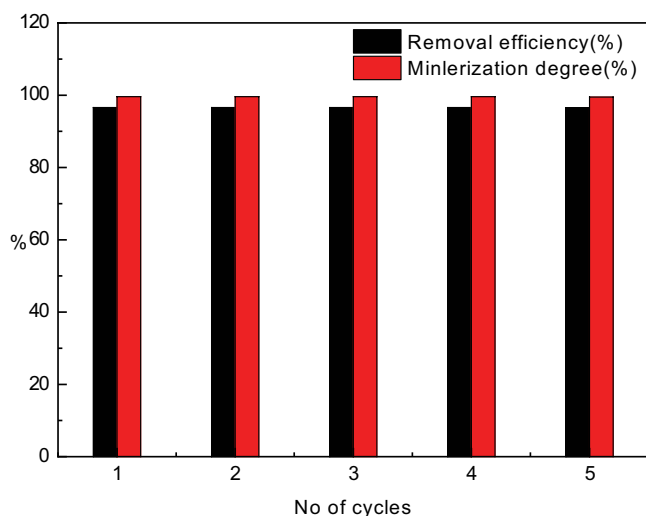


Fig. 10. Photocatalytic reuse of Fe/1C samples for remediation and mineralization of toluene for five times.

Whereas, hydroxyl radicals could be originated from both holes and electrons in the case of the FeWO_4 . And so, FeWO_4 could generate a greater quantity of hydroxyl radicals compared to those generated by $\text{g-C}_3\text{N}_4$.

3.2.2. Stability of photocatalysts

The stability of the fabricated specimens amid the gaseous toluene remediation actions has been tested via recycling examinations. Maximal remediation efficiency and mineralization extent of toluene via 1Fe/1C specimen after 5 rounds are exhibited in Fig. 10. It has been concluded that the photocatalytic destruction of gaseous toluene via 1Fe/1C was almost the same over 5 rounds. This finding proved the great stability of the fabricated specimens amid the toluene remediation.

4. Conclusion

Based on our investigation, the following conclusions could be derived:

- $\text{g-C}_3\text{N}_4$ and FeWO_4 were successfully associated to provide $\text{FeWO}_4/\text{g-C}_3\text{N}_4$ Z direct scheme arrangement for the photocatalytic destruction of gaseous toluene.
- Both $\text{g-C}_3\text{N}_4$ and FeWO_4 within the fabricated $\text{FeWO}_4/\text{g-C}_3\text{N}_4$ structure, might absorb Vis light needed for excitation of electrons from the V.B. to the C.B. and holes will be left in the V.B.
- As a result of the confidential assimilation between $\text{g-C}_3\text{N}_4$ and FeWO_4 , the photo-excited holes in the V.B. of the $\text{g-C}_3\text{N}_4$ could associate with the photo-excited electrons in the C.B. of the FeWO_4 leading to conservation of holes in the V.B. of the FeWO_4 and electrons in the C.B. of the $\text{g-C}_3\text{N}_4$.
- The fabricated $\text{FeWO}_4/\text{g-C}_3\text{N}_4$ arrangement could generate a definite quantity of accessible holes and electrons needed for the photocatalytic destruction of gaseous toluene especially beneath Vis light illumination.

- 1Fe/1C material showed the greatest photo-catalytic destruction efficacy amid all fabricated $\text{FeWO}_4/\text{g-C}_3\text{N}_4$ specimens.
- The maximal mineralization extent and remediation efficacy of gaseous toluene via 1Fe/1C were found to be 99.6% and 96.6%, respectively.
- The fabricated $\text{FeWO}_4/\text{g-C}_3\text{N}_4$ specimens displayed great stability towards the toluene remediation.

Acknowledgments

This project was funded by the Deanship of Scientific Research (DSR) at King Abdulaziz University, Jeddah, Saudi Arabia under grant no. KEP-MSc-3-130-40. The authors, therefore, acknowledge with thanks DSR for technical and financial support.

References

- [1] L. Zhong, J.J. Branco, S. Batterman, B.M. Bartlett, C. Godwin, Experimental and modeling study of visible light-responsive photocatalytic oxidation (PCO) materials for toluene degradation, *Appl. Catal., B*, 216 (2017) 122–132.
- [2] R. Xie, J. Ji, K. Guo, D. Lei, Q. Fan, D.Y.C. Leung, H. Huang, Wet scrubber coupled with UV/PMS process for efficient removal of gaseous VOCs: roles of sulfate and hydroxyl radicals, *Chem. Eng. J.*, 356 (2019) 632–640.
- [3] N. Zou, Q. Nie, X. Zhang, G. Zhang, J. Wang, P. Zhang, Electrothermal regeneration by Joule heat effect on carbon cloth based MnO_2 catalyst for long-term formaldehyde removal, *Chem. Eng. J.*, 357 (2019) 1–10.
- [4] C. Li, Z. Xi, W. Fang, M. Xing, J. Zhang, Enhanced photocatalytic hydrogen evolution activity of CuInS_2 loaded TiO_2 under solar light irradiation, *J. Solid State Chem.*, 226 (2015) 94–100.
- [5] T.-D. Pham, B.-K. Lee, C.-H. Lee, The advanced removal of benzene from aerosols by photocatalytic oxidation and adsorption of $\text{Cu-TiO}_2/\text{PU}$ under visible light irradiation, *Appl. Catal., B*, 182 (2016) 172–183.
- [6] T.D. Pham, B.K. Lee, Novel adsorption and photocatalytic oxidation for removal of gaseous toluene by V-doped TiO_2/PU under visible light, *J. Hazard. Mater.*, 300 (2015) 493–503.
- [7] M. Li, B. Lu, Q.-F. Ke, Y.-J. Guo, Y.-P. Guo, Synergetic effect between adsorption and photodegradation on nanostructured TiO_2 /activated carbon fiber felt porous composites for toluene removal, *J. Hazard. Mater.*, 333 (2017) 88–98.
- [8] T.-D. Pham, B.-K. Lee, Selective removal of polar VOCs by novel photocatalytic activity of metals co-doped TiO_2/PU under visible light, *Chem. Eng. J.*, 307 (2017) 63–73.
- [9] H. Mehrizadeh, A. Niaei, H.-H. Tseng, D. Salari, A. Khataee, Synthesis of ZnFe_2O_4 nanoparticles for photocatalytic removal of toluene from gas phase in the annular reactor, *J. Photochem. Photobiol., A*, 332 (2017) 188–195.
- [10] S. Boycheva, D. Zgureva, M. Václavíková, Y. Kalvachev, H. Lazarova, M. Popova, Studies on non-modified and copper-modified coal ash zeolites as heterogeneous catalysts for VOCs oxidation, *J. Hazard. Mater.*, 361 (2019) 374–382.
- [11] Y. Wang, D. Yang, S. Li, L. Zhang, G. Zheng, L. Guo, Layered copper manganese oxide for the efficient catalytic CO and VOCs oxidation, *Chem. Eng. J.*, 357 (2019) 258–268.
- [12] F.X. Prenafeta-Boldú, N. Roca, C. Villatoro, L. Vera, G.S. de Hoog, Prospective application of melanized fungi for the biofiltration of indoor air in closed bioregenerative systems, *J. Hazard. Mater.*, 361 (2019) 1–9.
- [13] Z. Shayegan, F. Haghghat, C.-S. Lee, Photocatalytic oxidation of volatile organic compounds for indoor environment applications: three different scaled setups, *Chem. Eng. J.*, 357 (2019) 533–546.
- [14] S. Fu, Y. Zheng, X. Zhou, Z. Ni, S. Xia, Visible light promoted degradation of gaseous volatile organic compounds catalyzed

- by Au supported layered double hydroxides: influencing factors, kinetics and mechanism, *J. Hazard. Mater.*, 363 (2019) 41–54.
- [15] T.D. Pham, B.K. Lee, P.C. De, Advanced removal of toluene in aerosol by adsorption and photocatalytic degradation of silver-doped TiO₂/PU under visible light irradiation, *RSC Adv.*, 6 (2016) 25346–25358.
- [16] R. Sun, Q. Shi, M. Zhang, L. Xie, J. Chen, X. Yang, M. Chen, W. Zhao, Enhanced photocatalytic oxidation of toluene with a coral-like direct Z-scheme BiVO₄/g-C₃N₄ photocatalyst, *J. Alloys Compd.*, 714 (2017) 619–626.
- [17] T.-D. Pham, B.-K. Lee, Photocatalytic comparison of Cu- and Ag-doped TiO₂/GF for bioaerosol disinfection under visible light, *J. Solid State Chem.*, 232 (2015) 256–263.
- [18] T.-D. Pham, B.-K. Lee, Novel integrated approach of adsorption and photooxidation using Ag-TiO₂/PU for bioaerosol removal under visible light, *Chem. Eng. J.*, 275 (2015) 357–365.
- [19] T.D. Pham, B.K. Lee, M.V. Nguyen, C.H. Lee, Germicide feasibility of TiO₂/glass fiber and Ag-TiO₂/glass fiber photocatalysts, *Adv. Mater. Res.*, 864 (2012) 518–523.
- [20] T.-D. Pham, B.-K. Lee, Advanced removal of *C. famata* in bioaerosols by simultaneous adsorption and photocatalytic oxidation of Cu-doped TiO₂/PU under visible irradiation, *Chem. Eng. J.*, 286 (2016) 377–386.
- [21] V.N. Nguyen, D.T. Tran, M.T. Nguyen, T.T.T. Le, M.N. Ha, M.V. Nguyen, T.D. Pham, Enhanced photocatalytic degradation of methyl orange using ZnO/graphene oxide nanocomposites, *Res. Chem. Intermed.*, 44 (2018) 3081–3095.
- [22] J. Tao, J.W. Chai, L.M. Wong, Z. Zhang, J.S. Pan, S.J. Wang, Growth of single crystalline TaON on yttria-stabilized zirconia (YSZ), *J. Solid State Chem.*, 204 (2013) 27–31.
- [23] N.T. Thanh Truc, N.T. Hanh, M.V. Nguyen, N.T.P. Le Chi, N. Van Noi, D.T. Tran, M.N. Ha, D.Q. Trung, T.-D. Pham, Novel direct Z-scheme Cu₂V₂O₇/g-C₃N₄ for visible light photocatalytic conversion of CO₂ into valuable fuels, *Appl. Surf. Sci.*, 457 (2018) 968–974.
- [24] D. Huang, Z. Li, G. Zeng, C. Zhou, W. Xue, X. Gong, X. Yan, S. Chen, W. Wang, M. Cheng, Megamerger in photocatalytic field: 2D g-C₃N₄ nanosheets serve as support of 0D nanomaterials for improving photocatalytic performance, *Appl. Catal., B*, 240 (2019) 153–173.
- [25] J. Xu, M. Fujitsuka, S. Kim, Z. Wang, T. Majima, Unprecedented effect of CO₂ calcination atmosphere on photocatalytic H₂ production activity from water using g-C₃N₄ synthesized from triazole polymerization, *Appl. Catal., B*, 241 (2019) 141–148.
- [26] N.T. Thanh Truc, L. Giang Bach, N. Thi Hanh, T.-D. Pham, N. Thi Phuong Le Chi, D.T. Tran, M.V. Nguyen, V.N. Nguyen, The superior photocatalytic activity of Nb doped TiO₂/g-C₃N₄ direct Z-scheme system for efficient conversion of CO₂ into valuable fuels, *J. Colloid Interface Sci.*, 540 (2019) 1–8.
- [27] B. Chai, C. Liu, J. Yan, Z. Ren, Z.-j. Wang, In-situ synthesis of WO₃ nanoplates anchored on g-C₃N₄ Z-scheme photocatalysts for significantly enhanced photocatalytic activity, *Appl. Surf. Sci.*, 448 (2018) 1–8.
- [28] Y. Tan, Z. Shu, J. Zhou, T. Li, W. Wang, Z. Zhao, One-step synthesis of nanostructured g-C₃N₄/TiO₂ composite for highly enhanced visible-light photocatalytic H₂ evolution, *Appl. Catal., B*, 230 (2018) 260–268.
- [29] Z. Yang, C. Deng, Y. Ding, H. Luo, J. Yin, Y. Jiang, P. Zhang, Y. Jiang, Eco-friendly and effective strategy to synthesize ZnO/Ag₂O heterostructures and its excellent photocatalytic property under visible light, *J. Solid State Chem.*, 268 (2018) 83–93.
- [30] Y. Gong, X. Quan, H. Yu, S. Chen, Synthesis of Z-scheme Ag₂CrO₄/Ag/g-C₃N₄ composite with enhanced visible-light photocatalytic activity for 2,4-dichlorophenol degradation, *Appl. Catal., B*, 219 (2017) 439–449.
- [31] M.-H. Wu, L. Li, Y.-C. Xue, G. Xu, L. Tang, N. Liu, W.-Y. Huang, Fabrication of ternary GO/g-C₃N₄/MoS₂ flower-like heterojunctions with enhanced photocatalytic activity for water remediation, *Appl. Catal., B*, 228 (2018) 103–112.
- [32] W. Zhang, X. Xiao, Y. Li, X. Zeng, L. Zheng, C. Wan, Liquid-exfoliation of layered MoS₂ for enhancing photocatalytic activity of TiO₂/g-C₃N₄ photocatalyst and DFT study, *Appl. Surf. Sci.*, 389 (2016) 496–506.
- [33] Y. Wang, W. Jiang, W. Luo, X. Chen, Y. Zhu, Ultrathin nanosheets g-C₃N₄@Bi₂WO₆ core-shell structure via low temperature reassembled strategy to promote photocatalytic activity, *Appl. Catal., B*, 237 (2018) 633–640.
- [34] M. Hao, X. Meng, Y. Miao, Synthesis of NiWO₄ powder crystals of polyhedron for photocatalytic degradation of Rhodamine, *Solid State Sci.*, 72 (2017) 103–108.
- [35] M. Eghbali-Arani, A. Sobhani-Nasab, M. Rahimi-Nasrabadi, F. Ahmadi, S. Pourmasoud, Ultrasound-assisted synthesis of YbVO₄ nanostructure and YbVO₄/CuWO₄ nanocomposites for enhanced photocatalytic degradation of organic dyes under visible light, *Ultrason. Sonochem.*, 43 (2018) 120–135.
- [36] W. He, Y. Sun, G. Jiang, H. Huang, X. Zhang, F. Dong, Activation of amorphous Bi₂WO₆ with synchronous Bi metal and Bi₂O₃ coupling: photocatalysis mechanism and reaction pathway, *Appl. Catal., B*, 232 (2018) 340–347.
- [37] M. Mousavi, A. Habibi-Yangjeh, Decoration of Fe₃O₄ and CoWO₄ nanoparticles over graphitic carbon nitride: novel visible-light-responsive photocatalysts with exceptional photocatalytic performances, *Mater. Res. Bull.*, 105 (2018) 159–171.
- [38] J. Zhang, Y. Wang, S. Li, X. Wang, F. Huang, A. Xie, Controlled synthesis, growth mechanism and optical properties of FeWO₄ hierarchical microstructures, *Cryst. Eng. Comm.*, 13 (2011) 5744–5750.
- [39] E.S. Babu, B.J. Rani, G. Ravi, R. Yuvakkumar, R.K. Guduru, V. Ganesh, S. Kim, Novel NiWO₄ nanoberry morphology effect on photoelectrochemical properties, *Mater. Lett.*, 220 (2018) 209–212.
- [40] M. Li, S. Yokoyama, H. Takahashi, K. Tohji, Bandgap engineering of NiWO₄/CdS solid Z-scheme system via an ion-exchange reaction, *Appl. Catal., B*, 241 (2019) 284–291.
- [41] I. Troppová, M. Šíhor, M. Reli, M. Ritz, P. Praus, K. Kočí, Unconventionally prepared TiO₂/g-C₃N₄ photocatalysts for photocatalytic decomposition of nitrous oxide, *Appl. Surf. Sci.*, 430 (2018) 335–347.
- [42] K. Kočí, M. Reli, I. Troppová, M. Šíhor, J. Kupková, P. Kustrowski, P. Praus, Photocatalytic decomposition of N₂O over TiO₂/g-C₃N₄ photocatalysts heterojunction, *Appl. Surf. Sci.*, 396 (2017) 1685–1695.
- [43] M.M.J. Sadiq, U.S. Shenoy, D.K. Bhat, NiWO₄-ZnO-NRGO ternary nanocomposite as an efficient photocatalyst for degradation of methylene blue and reduction of 4-nitro phenol, *J. Phys. Chem. Solids*, 109 (2017) 124–133.
- [44] Y. Wang, G. Tan, T. Liu, Y. Su, H. Ren, X. Zhang, A. Xia, L. Lv, Y. Liu, Photocatalytic properties of the g-C₃N₄/010 facets BiVO₄ interface Z-Scheme photocatalysts induced by BiVO₄ surface heterojunction, *Appl. Catal., B*, 234 (2018) 37–49.
- [45] Z. Mo, H. Xu, Z. Chen, X. She, Y. Song, J. Lian, X. Zhu, P. Yan, Y. Lei, S. Yuan, H. Li, Construction of MnO₂/Monolayer g-C₃N₄ with Mn vacancies for Z-scheme overall water splitting, *Appl. Catal., B*, 241 (2019) 452–460.
- [46] M. Mousavi, A. Habibi-Yangjeh, D. Seifzadeh, Novel ternary g-C₃N₄/Fe₃O₄/MnWO₄ nanocomposites: synthesis, characterization, and visible-light photocatalytic performance for environmental purposes, *J. Mater. Sci. Technol.*, 34 (2018) 1638–1651.
- [47] T.H. Do, C. Nguyen Van, K.-A. Tsai, L.T. Quynh, J.-W. Chen, Y.-C. Lin, Y.-C. Chen, W.-C. Chou, C.-L. Wu, Y.-J. Hsu, Y.-H. Chu, Superior photoelectrochemical activity of self-assembled NiWO₄-WO₃ heteroepitaxy, *Nano Energy*, 23 (2016) 153–160.
- [48] R. Lacomba-Perales, J. Ruiz-Fuertes, D. Errandonea, D. Martínez-García, A. Segura, Optical absorption of divalent metal tungstates: correlation between the band-gap energy and the cation ionic radius, *Europhys. Lett.*, 83 (2008) 37002.
- [49] J. Safaei, H. Ullah, N.A. Mohamed, M.F. Mohamad Noh, M.F. Soh, A.A. Tahir, N. Ahmad Ludin, M.A. Ibrahim, W.N.R. Wan Isahak, M.A. Mat Teridi, Enhanced photoelectrochemical performance of Z-scheme g-C₃N₄/BiVO₄ photocatalyst, *Appl. Catal., B*, 234 (2018) 296–310.
- [50] J. Meng, J. Pei, Z. He, S. Wu, Q. Lin, X. Wei, J. Li, Z. Zhang, Facile synthesis of g-C₃N₄ nanosheets loaded with WO₃ nanoparticles

- with enhanced photocatalytic performance under visible light irradiation, *RSC Adv.*, 7 (2017) 24097–24104
- [51] Y. Li, X. Wu, J. Li, K. Wang, G. Zhang, Z-scheme g-C₃N₄@Cs_xWO₃ heterostructure as smart window coating for UV isolating, Vis penetrating, NIR shielding and full spectrum photocatalytic decomposing VOCs, *Appl. Catal., B*, 229 (2018) 218–226.
- [52] Y. Xin, Q. Chen, G. Zhang, Construction of ternary heterojunction CuS-CdS/TiO₂ nanobelts for photocatalytic degradation of gaseous toluene, *J. Alloys Compd.*, 751 (2018) 231–240.
- [53] Y. Liu, L. Chen, Q. Yuan, J. He, C.T. Au, S.F. Yin, A green and efficient photocatalytic route for the highly-selective oxidation of saturated alpha-carbon C–H bonds in aromatic alkanes over flower-like Bi₂WO₆, *Chem. Commun.*, 52 (2016) 1274–1277.
- [54] B. Yuan, B. Zhang, Z.L. Wang, S.M. Lu, J. Li, Y. Liu, C. Li, Photocatalytic aerobic oxidation of toluene and its derivatives to aldehydes on Pd/Bi₂WO₆, *Chin. J. Catal.*, 38 (2017) 440–446.
- [55] H. Bai, W.C. Yi, J.Y. Liu, Q. Lv, Q. Zhang, Q. Ma, H.F. Yang, G.C. Xi, Large-scale synthesis of ultrathin tungsten oxide nanowire networks: an efficient catalyst for aerobic oxidation of toluene to benzaldehyde under visible light, *Nanoscale*, 8 (2016) 13545–13551.
- [56] L.N. Song, L. Chen, J. He, P. Chen, H.K. Zeng, C.T. Au, S.F. Yin, First synthesis of Bi self-doped Bi₂MoO₆-Bi₂Mo₃O₁₂ composite and its excellent photocatalytic performance for selective oxidation of aromatic alkanes under visible light irradiation, *Chem. Commun.*, 53 (2017) 6480–6483.